ISSN 0840-8440

PROCEEDINGS

TECHNOLOGY TRANSFER CONFERENCE 1988

November 28 and 29, 1988

Royal York Hotel

Toronto, Ontario

SESSION A
AIR QUALITY RESEARCH

Sponsored by

Research and Technology Branch

Environment Ontario

Ontario, Canada

A10

SCALE MODEL STUDIES AND DEVELOPMENT OF PREDICTION PROCEDURES FOR HEAVY GAS DISPERSION IN COMPLEX TERRAIN 1988

by

M.C. Murphy, K.C. Heidorn and P.A. Irwin

Rowan, Williams, Davies and Irwin Inc.

Guelph, Ontario

Presented at TECHNOLOGY TRANSFER CONFERENCE 1988, Toronto, Ontario

ABSTRACT

The overall goal of the "Heavy Gas Project" is to develop an improved computer model for the prediction of heavier-than-air gas dispersion in complex terrain.

Three basic areas of investigation comprise the Project: 1) experimental - zero wind releases; 2) experimental - releases into wind; and 3) mathematical modelling. In this paper we present our work on Part 1. More specifically, the spreading rate of a heavier-than-air gas cloud into a zero-wind environment is studied using flow visualization techniques. Smoke was used to follow the instantaneous release of a heavy gas onto firstly, a smooth level surface, and subsequently onto surfaces with obstacles arranged in different configurations. Overhead and side-view cameras were used tp photograph the spill events. Still photos were obtained from freeze-frame analysis of the video, and were then used to produce data on cloud front distance versus elapsed time.

Photos of the release showed a very uniform circular cloud spread onto a smooth surface. A release into obstacles appeared to start out initially as a uniform circular cloud, but at later times the cloud developed into a diamond or hexagonal shape, depending on the obstacle arrangement. Surprisingly, the cloud spreading rate was higher with obstacles present than for spreading on a smooth surface. This, however, was true only for cloud spreading through an open corridor in a uniform array of obstacles. A modified MOE model predicted the cloud spreading history with reasonable results.

Keywords: heavy gas, still-air, flow visualization, smooth, obstacles, model

1. INTRODUCTION

The widespread transport and storage of toxic and/or inflammable gases has increased interest in recent years in the behaviour of heavier-than-air gases released into the ambient atmosphere. In the event of a spill of a toxic or flammable heavy gas, an emergency response team must be able to respond quickly and efficiently to ensure that danger to the local community is minimized. This requires a real-time ability to predict the flow path and concentration pattern of the gas cloud for the duration of the spill event. In many cases, the gas is heavier than air, especially during the early stages of the release. The behaviour of the heavier-than air gas cloud depends on several variables such as local terrain roughness and slope, gas density, physical nature of the gas release (instantaneous, semi-continuous or continuous), spill rate and/or spill volume as well as weather conditions including wind speed and direction, atmospheric stability, precipitation, and humidity.

Perhaps the most important parameters in determining the behaviour of the gas cloud are gas volume and density, wind speed and direction and local terrain characteristics. The fact that weather conditions play a large role in heavy gas behaviour emphasizes the complex nature of the problem. Nevertheless, a large body of research has been, and is being, completed in an effort to help provide a quick and efficient response to a spill of toxic or inflammable heavy gases. Much of this work has been sponsored by industry and government in a approach similar to the joint venture at Thorney Island (McQuaid, 1985).

Research into heavier-than-air gas dispersion has proceeded on three fronts: 1) full-scale field trials, 2) wind tunnel simulations, and 3) theoretical prediction or computer simulation. Full-scale tests represent an enormous effort in manpower and funding. Wind tunnel and computer simulations are considerably less expensive and are very useful for validation purposes. In this study, the instantaneous release of a volume of heavy gas is simulated under zero-wind conditions and several different obstacle configurations. Similar tests are currently being carried out with non-zero wind, and these will be the subject of a later paper. Ultimately, the results of flow visualization and

concentration monitoring from these tests will be used to improve mathematical models of heavy gas dispersion.

In the first series of heavy gas dispersion experiments, a known volume of gas was released into a calm environment under a variety of obstacle arrays. For each of these releases, the flow of the gas cloud was observed and recorded on video tape. By varying the size and density of the obstacles as well as the initial cloud dimensions, the effects of these obstacles could be studied and then compared to simple box model predictions of the horizontal cloud dimensions. Improved mathematical expressions are proposed to describe the horizontal motion of the gas cloud in its early stages of dispersion.

2. EXPERIMENTAL PROCEDURES

The scale modelling of a heavy gas release consists of holding certain physical parameters constant for both the full scale and laboratory tests. Similarity criteria include the Reynolds (Re) and Froude (Fr) numbers based on wind velocity, Richardson number (Ri) based on wind velocity and density difference between gas spill and air, initial density ratio, volume and rate of release, wind velocity profile, surface roughness, turbulence (length scale and intensity) and weather stability class. The Reynolds number is given by:

$$Re = L\, U\, \delta_a / \mu \qquad (1)$$

where L is a length scale (arbitrarily defined), U is local wind velocity, δ_a is the air density, and μ is the viscosity. The Richardson number is:

$$Ri = g\, \Delta\delta / \delta_a\, L/U^2 \qquad (2)$$

where g is the gravitational constant, $\Delta\delta = \delta_g - \delta_a$, and δ_g is the gas density.

Not all criteria can be satisfied in practice. The Reynolds criteria cannot be satisfied for models at 1:500 scale because the velocity over the model

becomes very low, and it is difficult to obtain a good simulation of the boundary layer at low speeds in the wind tunnel. Fortunately, a reasonably complete simulation can be obtained, even in violation of Reynolds similitude (Meroney, 1982), (Meroney and Neff, 1986). This "non-exact" simulation can be established by ensuring that the Richardson number, Ri, is equal at both model and full scale. The density ratio may be increased in the model case so that the velocity on the model may be increased. This is done because a higher velocity simulation is much easier to perform.

The velocity profile over the model should be similar to the full scale wind profile. The absolute values of the velocities are obtained from Ri similitude. The surface roughness is scaled simply by geometric scaling. The turbulence intensity of the wind in the along-wind direction should be similar at model and full scale. In partial boundary layer simulation, some of these criteria may not be satisfied exactly. The velocity profile and surface roughness criteria are relatively easy to satisfy, but the length scale and turbulence intensity are more difficult. However, because the turbulence generated during the instantaneous release of a heavy gas spill is generally higher than atmospheric turbulence, exact similitude is not required. Thus, although the simulated boundary layer lacks some turbulent elements, the model spill will remain a reasonable representation of the full scale event.

The release mechanism developed for this study is illustrated in Figure 1. Design criteria included the following:

i) scale release volume;
ii) geometric shape;
iii) minimum interference from release;
iv) leak proof; and
v) flexible pull down mechanism.

Two release canisters were constructed to represent significantly different volumes of gas release. At 1:100 scale, the small canister (2000 cm^3) represented a Thorney Island release of 2000 m^3. The large canister (14000

cm^3) represented a 1:50 scale release. Figure 2 shows the release from the small canister into a zero-wind environment with no blocks. A small puff of smoke from the top of the release canister signals the beginning of the release, as shown in Figure 2-A. Less than 100 msec after the release, the cylinder disappears through the floor. The cloud remains cylindrical, is sheared uniformly along the sides, and begins to collapse before 100 msec. Figure 4-C and D show the overhead view of the spill. It can be seen that the spread of the cloud is uniform in all directions, indicating that the release mechanism was performing satisfactorily.

The gas used in the flow visualization study was Freon-12 mixed with carbon dioxide and smoke generated from mineral oil. By a careful weighing of a known volume of the Freon-CO_2-smoke mixture, the density of the heavy gas used in this study was found to be 3.89 kg/m^3.

The test arrays used in the initial flow visualization experiments resulted in 18 different test configurations which are defined in Table 1. Two block sizes were used: a small cube with 3.5 cm sides and a medium cube of 7 cm sides. Block coverage was either none, half or full. A schematic of full coverage is given in Figure 3. Half coverage has blocks only in the semicircle to the south of the canister location; and north of the canister there were no blocks (see North arrow on photos).

In most of the experiments using the cubes, the spacing of the blocks on the platform was 1:1 as shown in Figure 3. The 1:1 spacing indicates that the distances between the blocks (as indicated by E and D on Figure 3) is equal to the block width (as indicated by A and B on Figure 3). In two release series, a staggered spacing of 1:1 was used in which alternate rows are shifted one spacing to the left of the row below and above it. This spacing results in a 1:1 spacing within all rows and between the rows and a 1:3 spacing in each column. A 1:3 spacing indicates 3 block widths between adjacent blocks. In the regular 1:3 spacing, the blocks are so spaced in both the row and column directions.

Two canister sizes were also used in the release experiments. The small canister has a volume of 1995 cm^3, a height (indicated by G on Figure 3) of 12.5 cm and a diameter (F on Figure 3) of 14.1 cm. The large canister was 25.1 cm in diameter and 27.6 cm in height giving a volume of 13 615 cm^3.

In order to better scale the flow visualization records, two white tapes were located on model platform: one "above" and the other "below" the canister (e.g. see Figure 4). These tapes were located equidistant from the canister centre and were spaced 120.9 cm apart for the small canister and 192.7 cm apart for the large canister. In the later releases, the tapes were consistently placed 193 cm apart; white blocks were placed at the edge of the disk on the horizontal and vertical axes to facilitate the location of the canister centre (e.g. Figure 4).

For each obstacle array, the instantaneous release event was recorded on video tape by a camera mounted overhead. In several tests, a camera was also positioned to give a side view of the event. A digital time display added to the video tapes is seen in the upper corner of each of the photographs presented in this paper (e.g. Figure 4) and gives the time in hours, minutes, seconds and 1/30 second increments. In order to analyze the history of the cloud spread, the video tape was stopped at intervals and a photographic record made of the freeze-frame. These photographs were then used to determine the horizontal dimensions of the cloud at several instances after release.

3. FLOW VISUALIZATION OF STILL AIR RELEASES

In this first series of experiments, the horizontal spread of an instantaneous release of heavy gas under calm-wind conditions was simulated. Both the large and the small gas canisters were used in the flow visualization. Each canister offered desirable features in addition to the simulation of a number of different source/obstacle ratios. The large canister produced a more visible cloud than the small cylinder which facilitated tracking of the cloud front. The disadvantage of the large canister, however, is that its cloud reached the outer limits of the table much more quickly than the smaller

canister. The small canister thus allowed longer event observations; in many cases reaching the final passive stage of the heavy gas event for which the cloud no longer spreads primarily as a result of gravity forces.

The obstacle array and canister size variations for the 18-test series are presented in matrix form in Table 1. Brief discussions of those tests are given below. For ease in the discussion, the cloud will be described as a flat, two-dimensional figure with the "vertical" axis and direction indicated by the line running through the canister centre "up and down" on the photograph and the "horizontal" axis and direction taken as running "left and right" through the canister centre. Start times for the releases shown in these figures are given in Table 2 in hours, minutes, seconds and 1/30 second increments corresponding to the time signature shown in the individual photographs.

Test Series 8 and 9 were run with no obstacles and with the small and large canisters respectively. In both cases, the heavy gas cloud spread in a circular manner as expected with the radius of the cloud increasing with time. The comparison of these clouds at an equal time after release is shown in Figure 4. It should be noted that the clouds are nearly perfect circles indicating that the experimental surface is very level and that there is no major influence by the release mechanism on the cloud dispersion. The upper photographs in Figure 4 are of the cloud at 0.33 seconds after release and the lower photographs are from 1.00 seconds after release. As expected, the cloud from the large canister has a larger radius than the cloud from the small canister after an equal time interval. It is also interesting to note the very visible outer "halo" at the cloud front and the thinner cloud density within the ring. (The bright inner circle is due to reflection from the release mechanism pad.)

Series 1, 2, 5, 6 and 10 were run with full coverage (sheets of blocks both to the north and to the south of the canister) using both the small blocks and the medium blocks with the small and large canister releases. (See Table 1 for each setup for these series.) All of these runs are characterized by a cloud pattern which initially begins as a circular shape but soon transforms into a diamond pattern with apices at the "north-south" and "east-west" axes through the cylinder centre. An example of this flow pattern is given in Figure 5 for the large canister and medium blocks. The start time for this series was at 03:40:00. As with the "no blocks" cases, the large canister cloud moves more quickly than that from the small canister (photos of small canister release not shown).

Series 3, 4 and 7 were trials with "half coverage", i.e. blocks only on the southern half of the study platform. (See Table 1 for configuration details.) We see that the cloud patterns (Figure 6) generated by this configuration are half like the "no blocks" case and half like the "full coverage" case: a semicircle to the north and a half-diamond to the south. In the early life of the cloud, the spread is in a nearly perfect circular pattern with cloud front movement through the blocks as rapid as that in the block-free half. The most surprising result of these trials is that the rate of spread of the cloud front is the same along the circle radii as it is along the apex of the diamond in the southern half. This similar rate of spread is found to occur regardless of the canister or block size. The indication is that, for this half-coverage configuration, a heavy gas cloud will flow along an unobstructed corridor between obstacles at the same rate as it would if no obstacles were present. Further discussion of this phenomenon will be given in the next section.

Series 11 and 12 were trials using half and full coverage of medium-size blocks with 1:1 spacing and the large canister release. The difference between these two series and Series 4, 5 and 10 is that the alternate rows of blocks are staggered by one block width. With this arrangement for the full coverage case, the open corridors along the north-south axis no longer exists. The arrangement does, however, still have an open east-west axis. The initial cloud spreads as a circle (Figure 7) and then transforms into a hexagon pattern. The half-coverage configuration results in an arrangement with a half-hexagonal pattern to the south and semi-circle to the north (Figure 8). The point of interest in these series is that the apices of the hexagon in the southern half (and in the northern half, in the case of full coverage) can be seen to occur in a diagonal direction from the release area, a path which is free of intersections

with any blocks. The movement along the north-south axis, however, is now impeded by the blocks and thus is slowed. The distance travelled from the canister centre to the centre points of the hexagon faces is essentially equidistant in all directions once the figure is established. The hexagon is elongated along the east-west axis as the cloud moves along the corridor free of impediment as it did in the regular array case.

Series 15 and 16 consist of a heavy gas spill with the large and small canisters for full coverage of medium blocks at a 1:3 spacing. Again, the spread begins as a circle (Figure 9) and remains nearly circular although there is the hint of a diamond shape in the later times with the large canister. The edges of the cloud front are seen to be "scalloped" around the obstacles indicating the flow pattern around the blocks.

Series 17 and 18 were run with the large canister and medium blocks with 2 cm-spacing (3.5:1 spacing) for full and half coverage respectively. Because of the narrowness of the corridors between blocks, some of the gas "sloshes" over the blocks upon release and forms a secondary cloud above the blocks. The pattern is further complicated by a rebound of the gas from the blocks. This process is dramatically seen in a series of scenes taken of the release region with a hand-held video camera (Figure 10). The cloud is seen to break over the blocks, initially clearing the floor of the canister. The gas then returns to fill the release area and a second wave is formed. This process is repeated with ever-diminishing strength. A side view of the process from a wider angle is shown in Figures 11 and 12. Very evident from this series is the secondary cloud spreading over the top of the blocks. This upper level cloud is evident from the overhead photographs (Figure 13) as a brightening and obscuration of the block tops. The horizontal pattern initially spreads as a diamond and likely continues to spread in that pattern although the gas becomes difficult to see in the corridors after some time. The cloud moving over the blocks hints at a four-pointed star pattern which evolves toward a hexagon.

For the half-coverage case (Figure 14), the clear-area semi-circle is present with a diamond shape evolving in the corridors between the blocks. The initial overflow of the blocks is evident as a rectangular bright area which quickly dissipates. Since the rebounding material has open terrain ahead of it, there is no back-and-forth slosh as there was with the complete coverage.

Series 13 and 14 were trials using simple solid barriers. In one, a pair of barriers were angled at 45 degrees and spaced so that a gap existed between them. In the other, a single barrier was placed horizontally. The cloud front was unaffected in all directions except where it touched the barrier which stopped the cloud front. The cloud wrapped around the barriers and would eventually fill in the space behind. Figure 15 shows these releases about a second after release.

4. ANALYSIS OF FLOW VISUALIZATION RESULTS

The flow visualization experiments provided a good record for analyzing the movement of the heavy gas cloud after its release. By reducing the videotape record to a series of photographs, the horizontal dimensions of the cloud could be determined and a time/distance history of the cloud front under a variety of release conditions ascertained. This was accomplished by measuring the distance on an enlargement of the photograph of various points along the cloud front from the canister centre and scaling the result by the known distance between the horizontal tapes above and below the canister.

The error in the measurement of points on the cloud front was ±0.5 mm from the photographs. The scale factor, between the photograph and the model, ranged from 22 to 25. Thus, the actual error in the placement of the cloud front is 1.1 cm to 1.3 cm. The clock used resolved time into increments of 1/30 of a second.

The distance of the cloud front from the canister centre as a function of elapsed time is shown in Figure 16 for both the large and small canisters under "no blocks" configurations. As expected, flow from the large canister

spread at a faster rate than from the small canister. The solid lines represent the current MOE model with coefficient equal to unity. Modelling, including the definition of the coefficient, is discussed in detail in the next section.

In this paper, only the 1:1 regular block spacing has been analyzed for cloud spread. For the large canister, the cloud front distance as a function of elapsed time is shown in Figures 17 and 18 for a variety of block size and coverage configurations. Figure 17 shows the distance measured along the axes (90 degrees) and Figure 18 shows the distance as measured at a 45 degree angle through the blocks. Similarly, Figure 19 (90 degrees) and Figure 20 (45 degrees) show measured distances for the small canister under several block configurations.

When compared with the configurations with blocks, the frontal distances for large canister releases along the axes for the "no blocks" configuration are less than distances measured with blocks present as full coverage (Figure 17). In other words, the cloud front moves faster with blocks present than without, at least along the corridors, and this holds for full coverage and no-blocks configurations only. Despite some scatter in the data, there is a distinct pattern of the distances aligning in relation to the block configuration. The distance travelled after a given time, i.e. the cloud spread, is seen to increase in the following sequence of block patterns: no blocks, medium blocks-half coverage, medium blocks-full coverage, small blocks-full coverage. The spread of the cloud from the small canister, however, shows only a slight differentiation between configurations with the "no blocks" spread being marginally faster (Figure 19). The velocity difference between configurations may be due to the different combinations in the source size, obstacle size and obstacle spacing but how the process evolves has not yet been fully determined. It is interesting to note that, in the half-coverage cases, the rate of spread along the north-south axes, through blocks on southern half and open in northern half, is virtually identical. For full block and no block coverage, the reason is obvious, the symmetry of obstacle placement. However, why this holds also for the half coverage cases is also not yet understood.

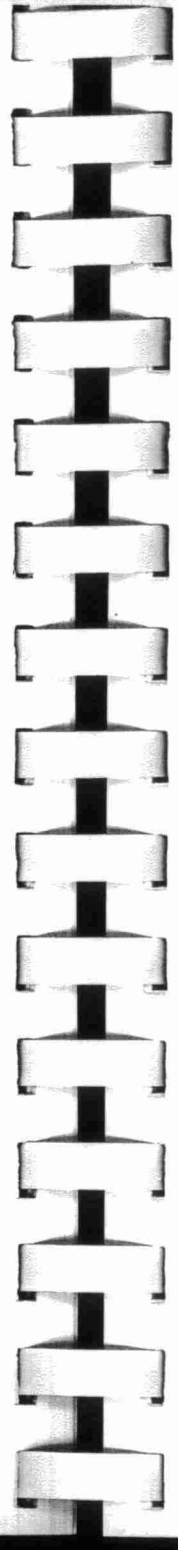

The distances travelled along the 45 degree paths (Figures 18 and 20) do not show a distinct pattern among block configurations, during the initial stages of the spill. In later stages, however, the rate of spread was higher for the "no-blocks" configuration. This difference in spreading rate seems to distinguish a transition from a circular spreading pattern (initial stage) to a diamond spreading pattern (next stage). The transition occurs earlier for a large canister release (0.6 - 1.0 seconds) than for the small canister release (1.0 - 1.5 seconds). This was expected because of the higher pressure head afforded by the large canister.

5. MODELLING OF HORIZONTAL CLOUD SPREAD

The atmospheric dispersion of heavy gases cannot be described fully by general gas dispersion methods. Mathematical models which treat the gravity spreading of a heavy gas cloud and the entrainment of ambient air into the cloud have been developed by a number of investigators over the past two decades. An excellent review was presented by Havens (1982). The modelling of an instantaneous heavy gas release is generally considered to be comprised of three phases. The first phase is the "blow-up" phase where the gas is initially released into the environment. The second phase is the "initial spreading" phase where the cloud moves as a slumping column of nearly uniform gas which mixes via turbulent entrainment of ambient air. The second phase ends and the third phase begins when the density difference between the cloud and ambient becomes sufficiently small. In this third phase, the gas cloud is sufficiently dilute that its dispersion may be treated by the traditional puff dispersion theories.

We consider here the initial stages of the second phase. It is assumed that the result of the gas release is a cylindrical cloud of known dimensions. Using a simple box model approach to heavy gas dispersion (MOE, 1983), the gas slumping phase is assumed to be controlled by gravitational effects. Assuming a constant cloud volume during this phase gives the following relationship for the rate of spread of the cloud under still air conditions:

$$r^2 = r_o^2 + 2Ct[\Delta\delta/\delta_a g V_o/\pi]^{1/2} \quad (3)$$

where r is the cloud radius at time t, r_o is the initial cloud radius at t=0, C is a constant, $\Delta\delta = \delta_g - \delta_a$, δ_g and δ_a are the gas and air densities respectively, V_o is the initial gas volume, and g is the gravitational constant.

In theory, the constant C could be either 1 or 1.414 (Hoult, 1972), but experimental results have shown C=1 to be the better choice (van Ulden, 1974; de Nevers, 1984). We next consider the value of C in light of our data.

Applying equation (3), with C=1, to the experimental data from the "no blocks" case (presented in Figure 16) results in a slight under prediction of the distance to the cloud front. (Note the lines in Figure 16 refer to the model values). The model consistently underpredicts the cloud radius for both canisters. In order to improve the model fit, the constant C was determined empirically through (3) for each time segment and the resulting values averaged. Under the "no block" configuration for the large canister, the average value of C was found to be 1.19. When this value for C is used in (3), the lower curve on Figures 17 results. The upper set of points in Figure 17 are the results of the "small block-full coverage" scenario. The value for C calculated for this configuration is 1.75, and a plot of (3) using this value of C is shown as the upper solid curve in Figure 17. A value of C=1.54 which is an average of all values of C from all large canister releases with blocks gives a line (not shown) midway between the two extremes.

For the small canister releases, the value of C determined from several different configurations ranges between 1.24 and 1.27. Only the plot of (3) with C=1.27 is shown on Figure 19.

From these physical model experiments, the "constant" C in equation (3) is found to vary with release size and, for the large release, with the obstacle configuration. We next consider whether this constant can be related to block size or spacing.

In those releases with a regular 1:1 block array, the heavy gas cloud was observed to begin as a circular cloud and then take on a diamond shape as it moved through the blocks. This flow regime shows the portion of the cloud moving down the unobstructed corridors between the blocks along the two horizontal axes to be spreading the quickest while the flow on the 45^o pathway moves slowest after an initial period of equal speed. From the geometry of the final configuration, a simple model of the flow regime is proposed to be:

$$r_d = r\ f(t) \quad (4)$$

where r_d is the distance of spread from the canister centre, r is the distance calculated by (3) down the axes, f(t) is the shape factor as a function of time t. Note f(t) is defined as:

$$f(t) = [\sin 45/\sin(135-\alpha)][e^{-\beta t}\{\sin(135-\alpha)/\sin 45\} + (1-e^{-\beta t})] \quad (5)$$

where α is the angle (in degrees) of the radius from the horizontal axis and β is a factor which is equal to 1 for blocks and 0 for no blocks. Note that for $\beta = 0$, $f(t) \rightarrow 1$, and equation (4) becomes $r_d = r$, i.e. the equation of a circular cloud front. With $\beta = 1$, as $t \rightarrow \infty$, equation (5) reduces to $\sin(45)/\sin(135-\alpha)$. Equation (4) then describes a linear cloud front connecting the two maximum radii at $\alpha=0^o$ and 90^o. Figures 18 and 20 show the results of this model for the 45^o radius for the large and small canisters respectively. In Figure 18, the distance was calculated using C=1.54, the value which gave the best fit for all the block data.

The mathematical model for heavy gas cloud radius (gas cloud spread) as a function of time given by (4) provides a good fit to the measured cloud dimensions under calm winds for dispersion though a regular array of blocks as well as the "no blocks" situation. This model is similar in form to the gravitational spread models proposed by many authors (e.g. van Ulden, 1974; MOE, 1983; de Nevers, 1984) with the "constant" term, generally taken as 1, increased to between 1.19 and 1.75 depending upon the obstacle configuration.

This very specific approach of fitting data must be generalized to incorporate other types of complex terrain. As more data become available, two approaches may be considered. Firstly, data from several different terrain types may be fitted to a specific model, where for each terrain type a different set of empirical constants are recommended. This leaves the end user to make a judgement on the terrain type. A second approach is to determine a set of empirical constants averaged over all terrains tested, and including the error band. The end user can than use the error bands in making judgements on the cloud path. In subsequent work we shall look at both approaches in light of wind tunnel data on heavy gas concentration measurements.

6. CONCLUSIONS AND FUTURE WORK

The flow visualization experiments for an instantaneous heavy gas released in an array of regularly spaced obstacles have resulted in a number of interesting spread patterns. The analysis of the visual record of these releases has given a cloud spread history for each of the various configurations which has been used to test a basic mathematical model of cloud radius under gravitational spreading. The results of that comparison indicate that the models fit the observations well when an empirical constant is introduced.

The next step in this study is to measure the gaseous concentration at a number of locations and to expand the gas spread model to predict concentrations. In addition, other release conditions will be studied including the non-zero wind case..

REFERENCES

de Nevers, N. (1984) 'Spread and Down-Slope Flow of Negatively Buoyant Clouds', Atmos. Environ., 18:2023-2027.

Havens, J.A. (1982) 'A Review of Mathematical Models for Prediction of Heavy Gas Atmospheric Dispersion', I.Chem.E. Symp. Series NO. 71:1-24.

Hoult, D.P. (1972) 'Oil Spreading on the Sea', Ann. Rev. Fluid Mech. 4:341-368.

McQuaid, J., ed. (1985) 'Heavy Gas Dispersion Trials at Thorney Island', Chem. Eng. Monograph, Vol. 22, Elsvier, 435pp.

Meroney, R.N. (1982) 'Wind tunnel experiments on dense gas dispersion', in 'Dense Gas Dispersion', Britter, R.E. and R.F. Griffiths, Chem. Eng. Monograph v16, pp. 85-106.

Meroney, R.N. and D.E. Neff (1986) 'Heat transfer effects during cold dense gas dispersion: wind tunnel simulation of cold gas spills', J. Heat Transfer, v108, p9-15.

MOE (1983) 'Portable Computing System for Use in Toxic Gas Emergencies', Ontario Ministry of the Environment Report ARB-162-83-ARSP, Toronto.

van Ulden, A.P. (1974) 'On the Spreading of a Heavy Gas Released Near the Ground', 1st Int'l Loss Prevention Symp., The Hague/Delft. Elsevier, Amsterdam, p221-226.

TABLE 1

TEST SERIES CONFIGURATIONS

Test Series Number	Canister Size	Block Size	Block Spacing	Block Coverage
1	L	S	1:1	Full
2	S	S	1:1	Full
3	S	S	1:1	Half
4	L	M	1:1	Half
5	L	M	1:1	Full
6	S	M	1:1	Full
7	S	M	1:1	Half
8	S	-	-	None
9	L	-	-	None
10	L	M	1:1	Full
11	L	M	1:1	Full Staggered
12	L	M	1:1	Half Staggered
13	L	-	-	2 Barriers, 45°
14	L	-	-	1 Barrier
15	L	M	1:3	Full
16	S	M	1:3	Full
17	L	M	3.75:1	Full
18	L	M	3.75:1	Full

Legend: Canister Size: S - small; L - large
Block Size: S - small; M - medium

TABLE 2

START TIME FOR EXAMPLE RELEASES IN PHOTO SEQUENCES

Figure Number	Start Time
2	01:23:36:05
4a	00:03:24:05
4b	00:02:42:20
5	00:03:40:00
6	00:03:57:15
7	00:08:37:20
8	00:09:17:05
9	00:08:18:00
10	
11	00:04:51:11
12	00:04:51:11
13	00:04:14:20
14	00:05:44:15
15a	
15b	

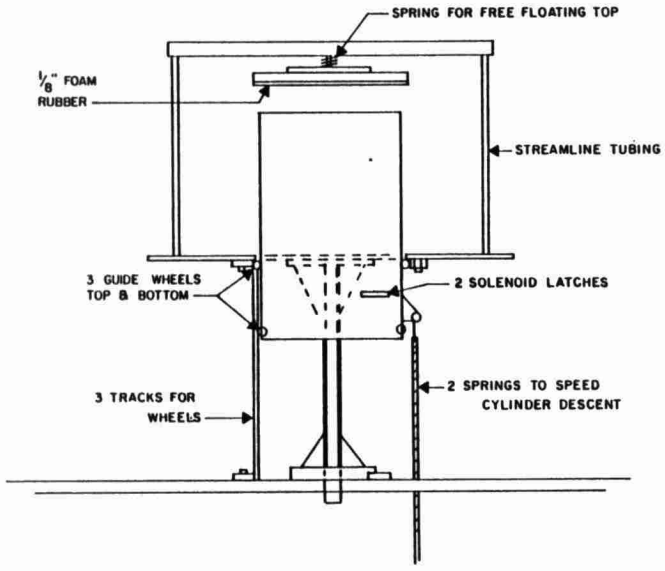

FIGURE 1
RELEASE MECHANISM SCHEMATIC

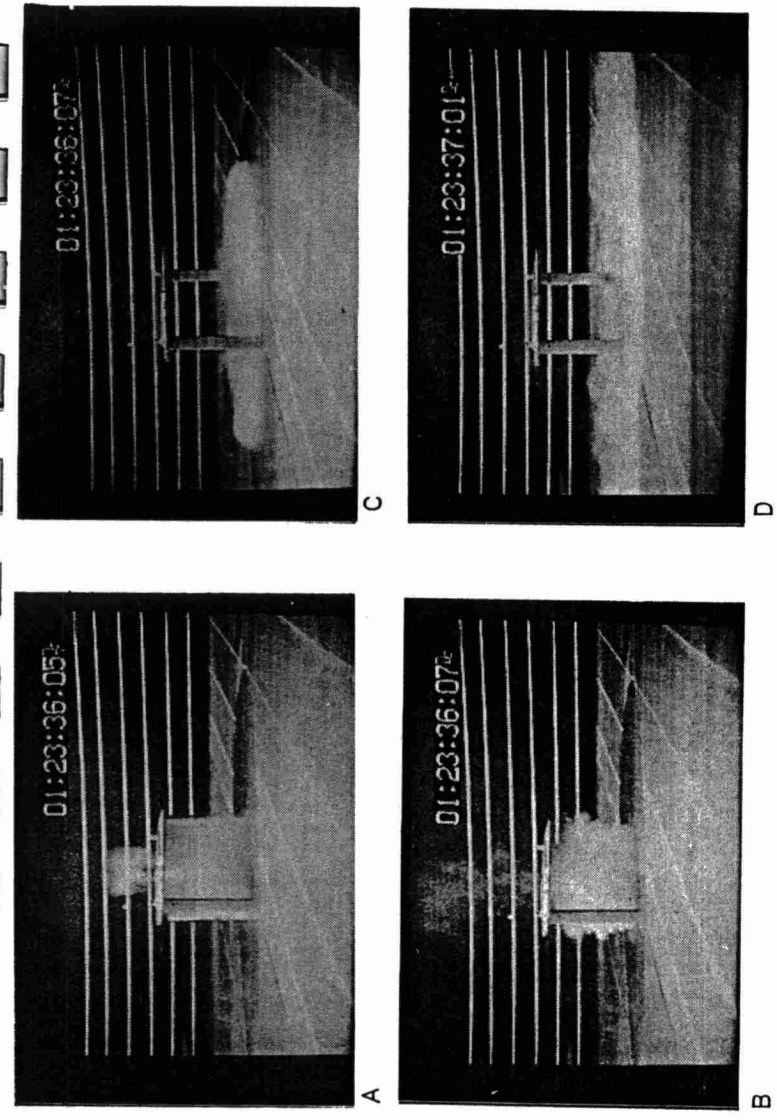

FIGURE 2
HEAVY GAS RELEASE MECHANISM

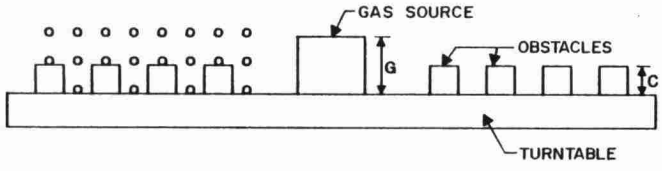

PROFILE VIEW

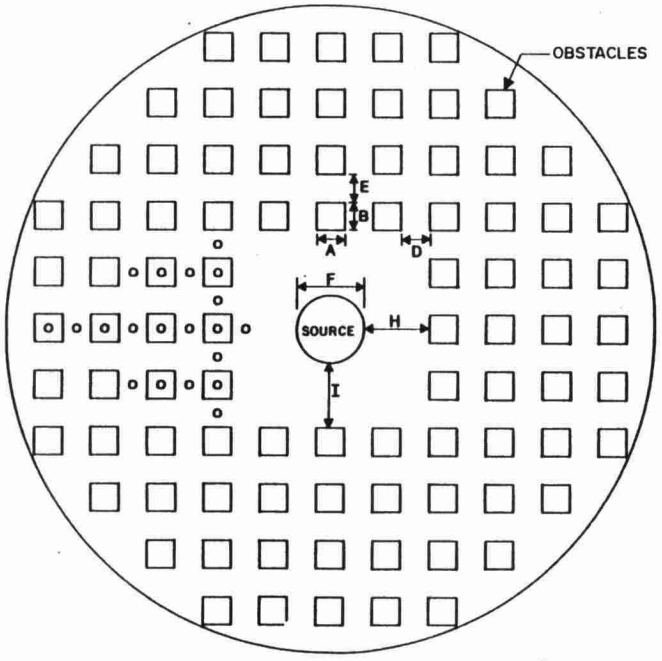

PLAN VIEW

o INDICATES SENSOR LOCATION

FIGURE 3
UNIFORM TERRAIN IN THE WIND TUNNEL

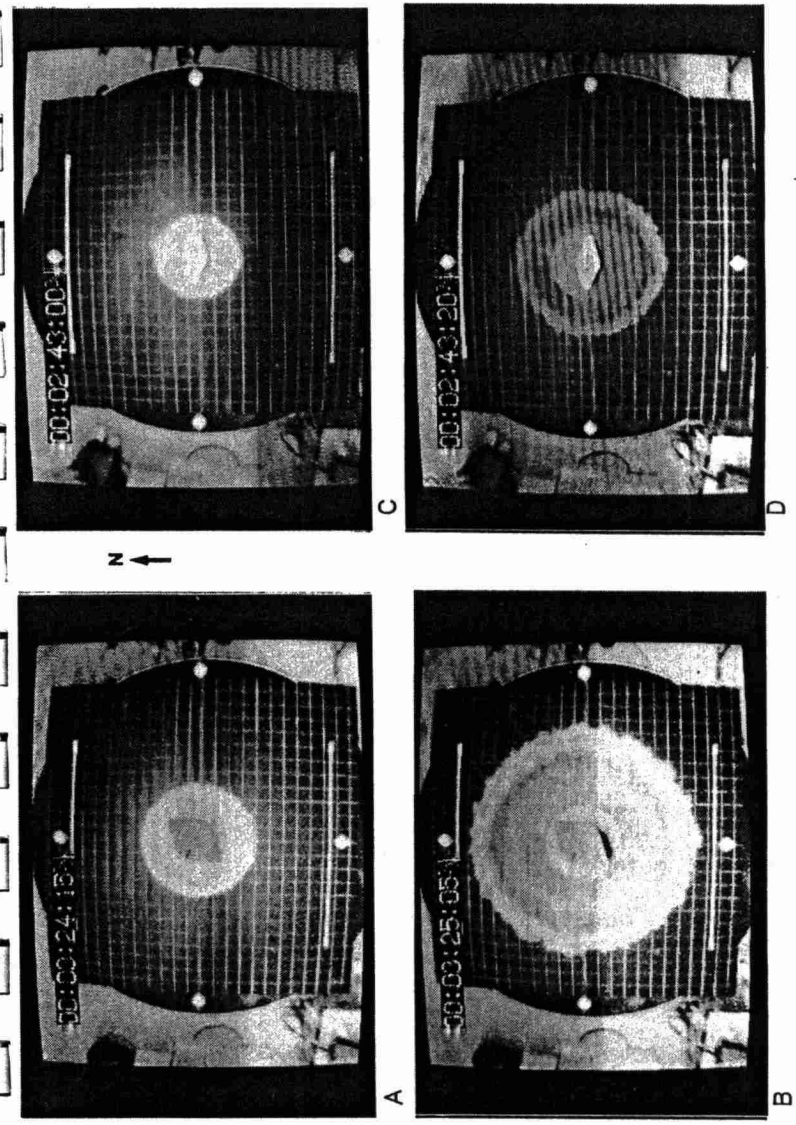

FIGURE 4
OVERHEAD VIEW OF HEAVY GAS RELEASE: NO OBSTACLES
A & B LARGE CANISTER C & D SMALL CANISTER

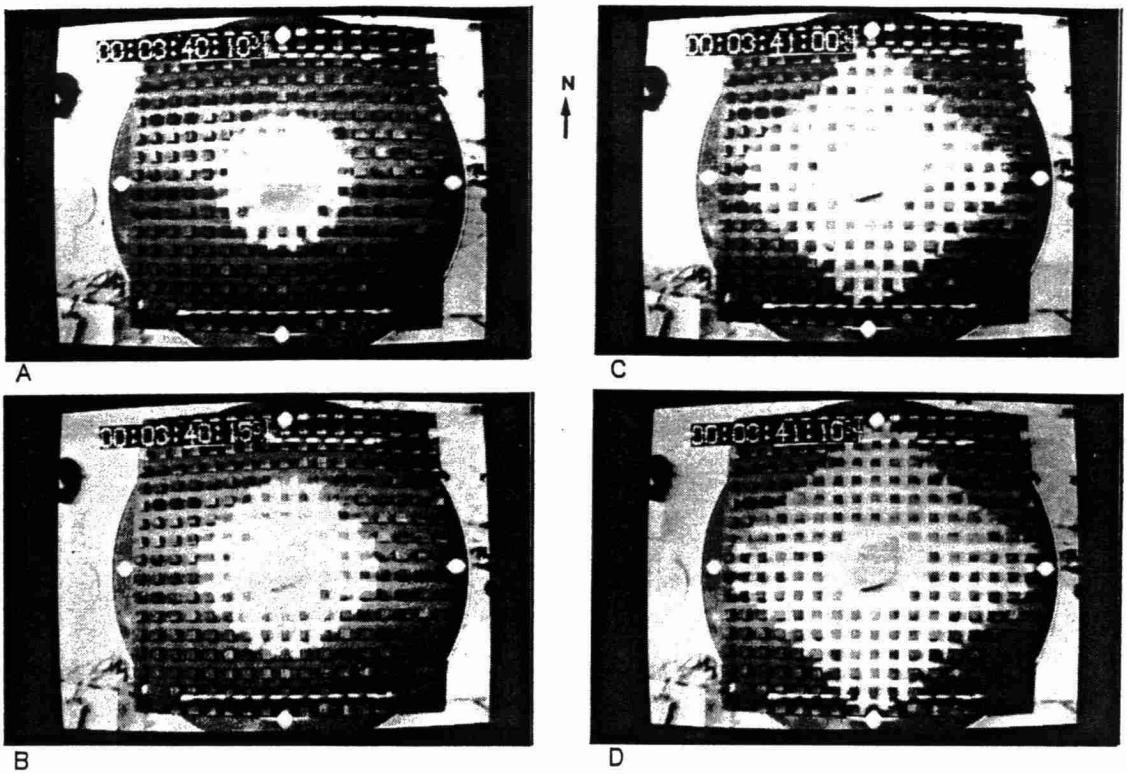

FIGURE 5
OVERHEAD VIEW OF HEAVY GAS RELEASE: LARGE CANISTER,
MEDIUM BLOCKS, 1:1 SPACING, FULL COVERAGE

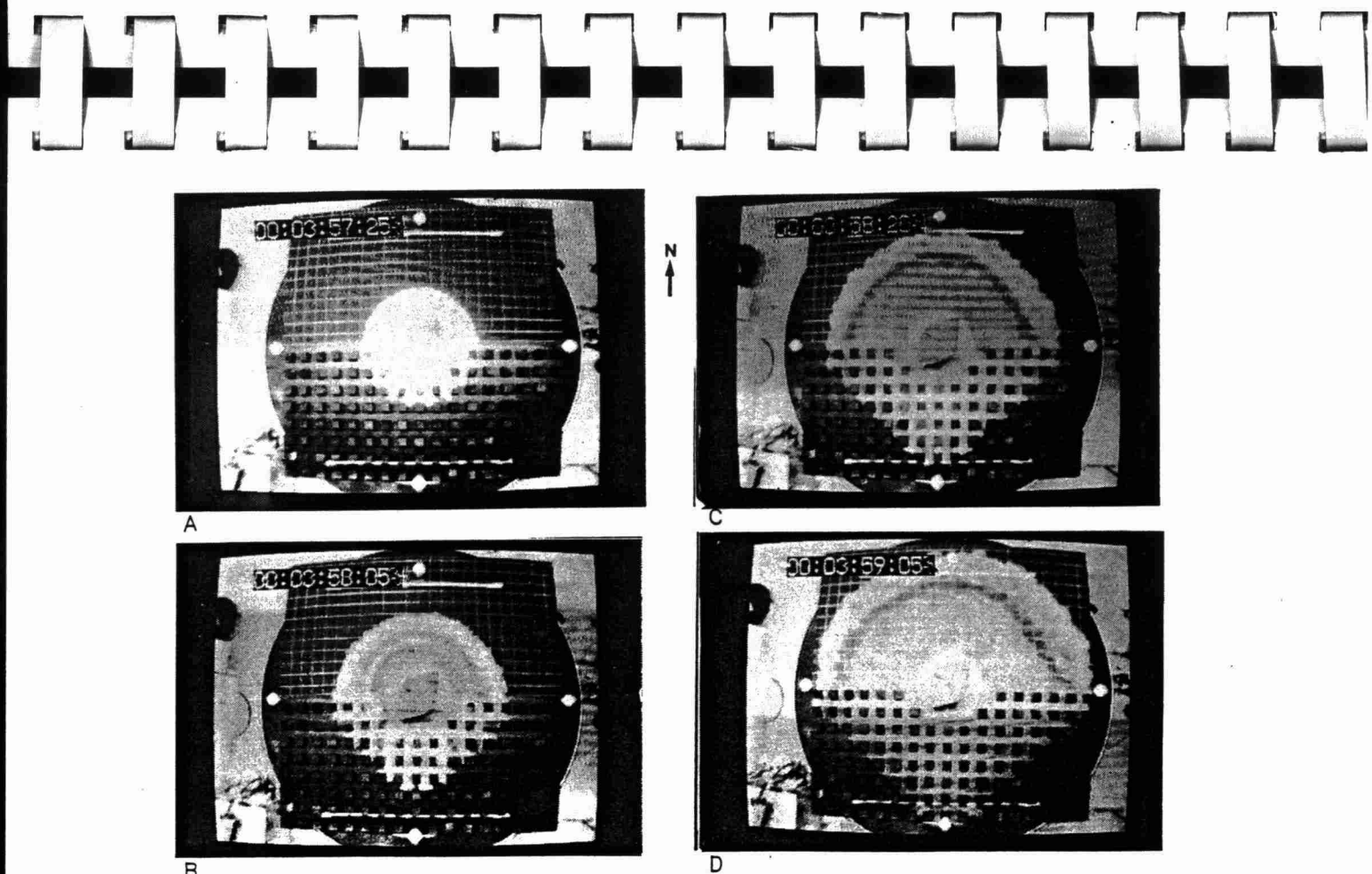

FIGURE 6
OVERHEAD VIEW OF HEAVY GAS RELEASE: LARGE CANISTER,
MEDIUM BLOCKS, 1:1 SPACING, HALF COVERAGE

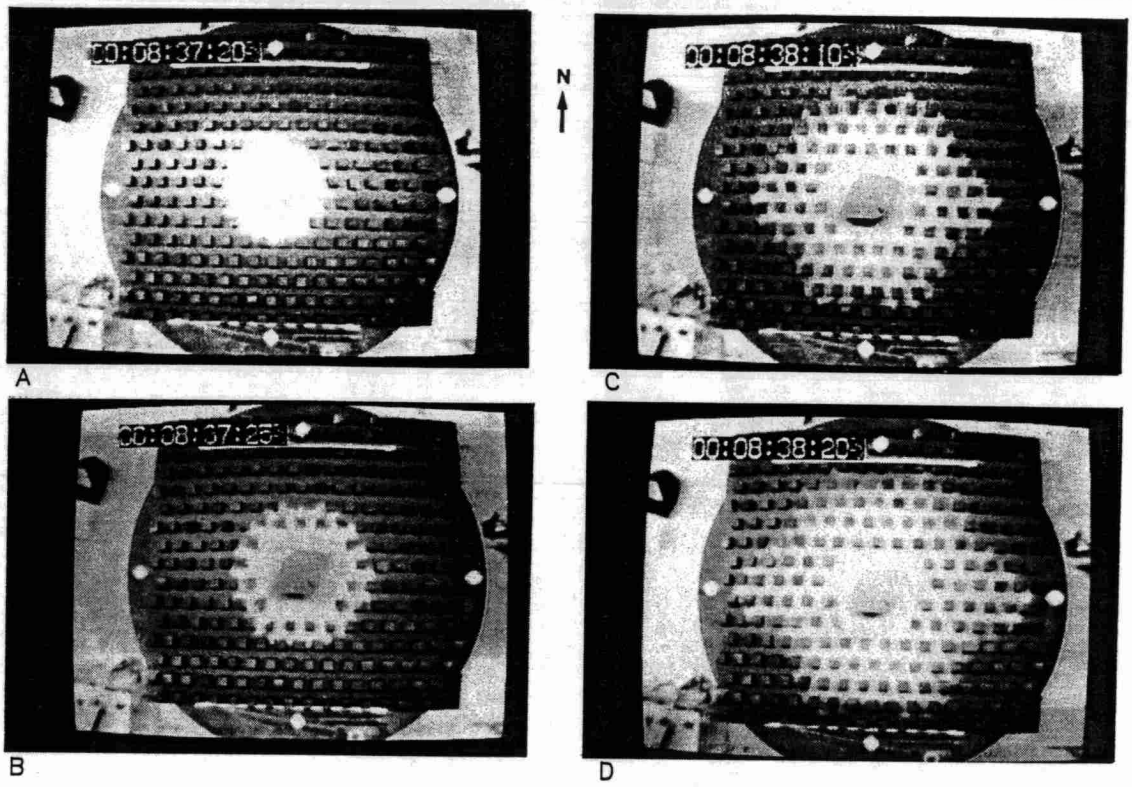

FIGURE 7
OVERHEAD VIEW OF HEAVY GAS RELEASE: LARGE CANISTER, MEDIUM BLOCKS, 1:1 STAGGERED SPACING, FULL COVERAGE

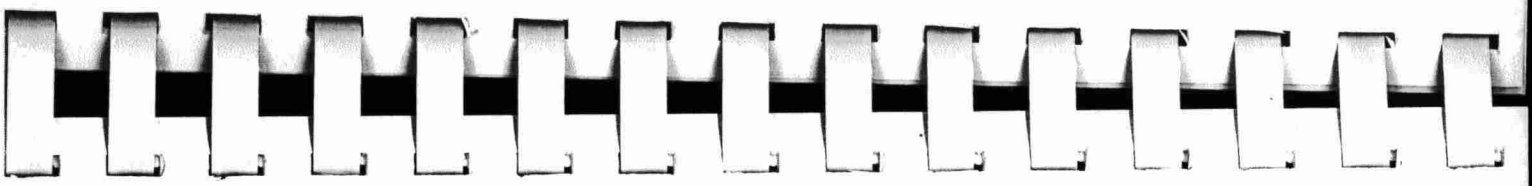

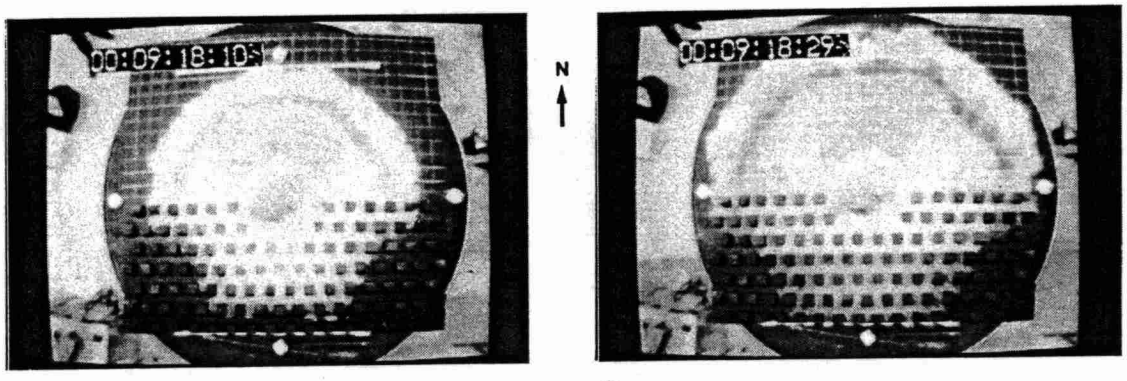

FIGURE 8
OVERHEAD VIEW OF HEAVY GAS RELEASE: LARGE CANISTER, MEDIUM BLOCKS, 1:1 STAGGERED SPACING, HALF COVERAGE

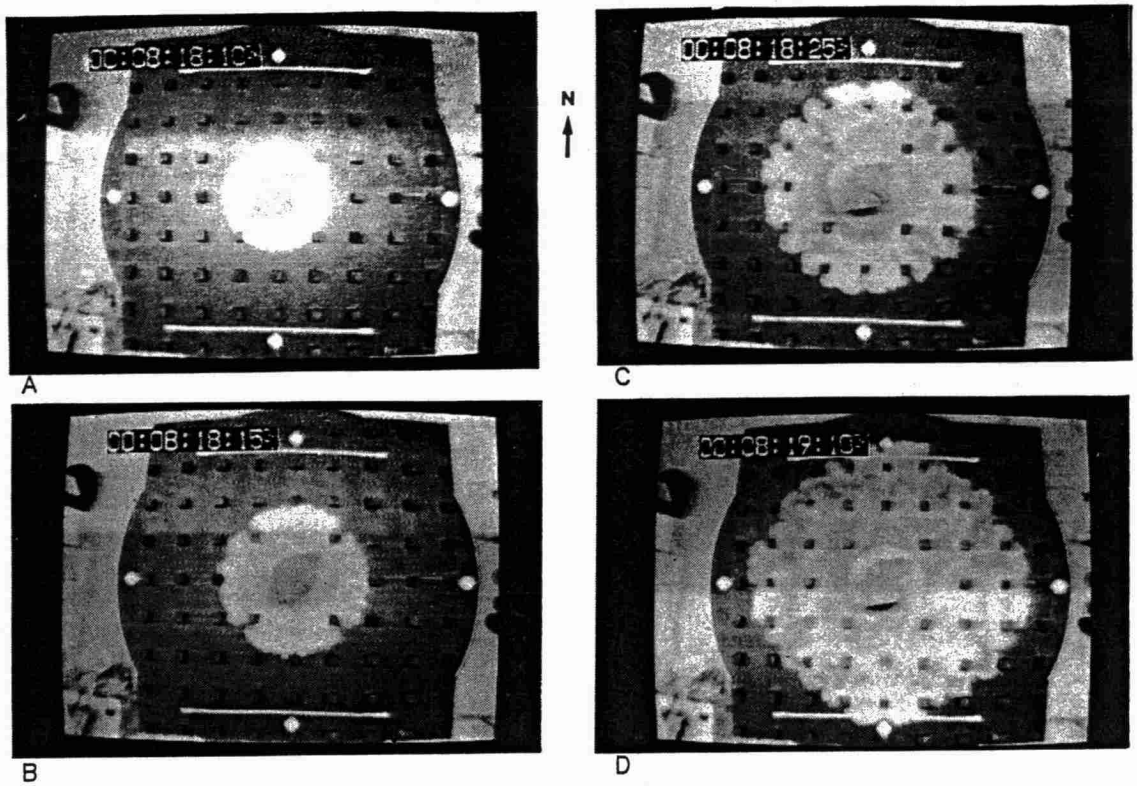

FIGURE 9
OVERHEAD VIEW OF HEAVY GAS RELEASE: LARGE CANISTER,
MEDIUM BLOCKS, 1:3 SPACING, FULL COVERAGE

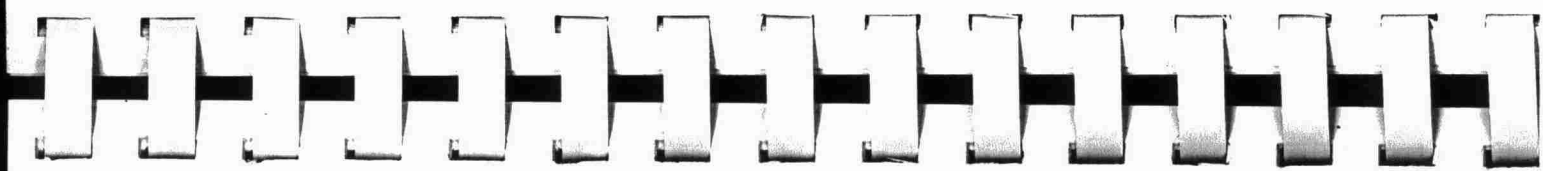

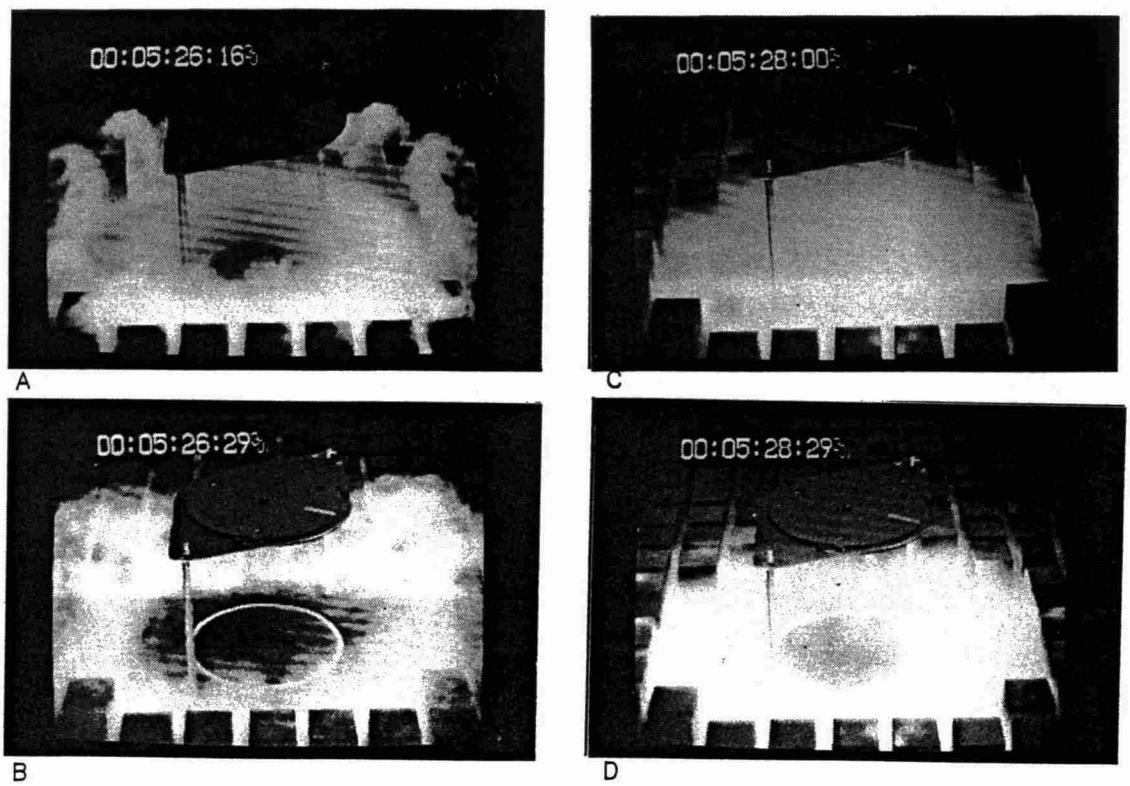

FIGURE 10
RELEASE AREA FOR HEAVY GAS RELEASE: LARGE CANISTER,
MEDIUM BLOCKS, 3.5:1 SPACING, FULL COVERAGE

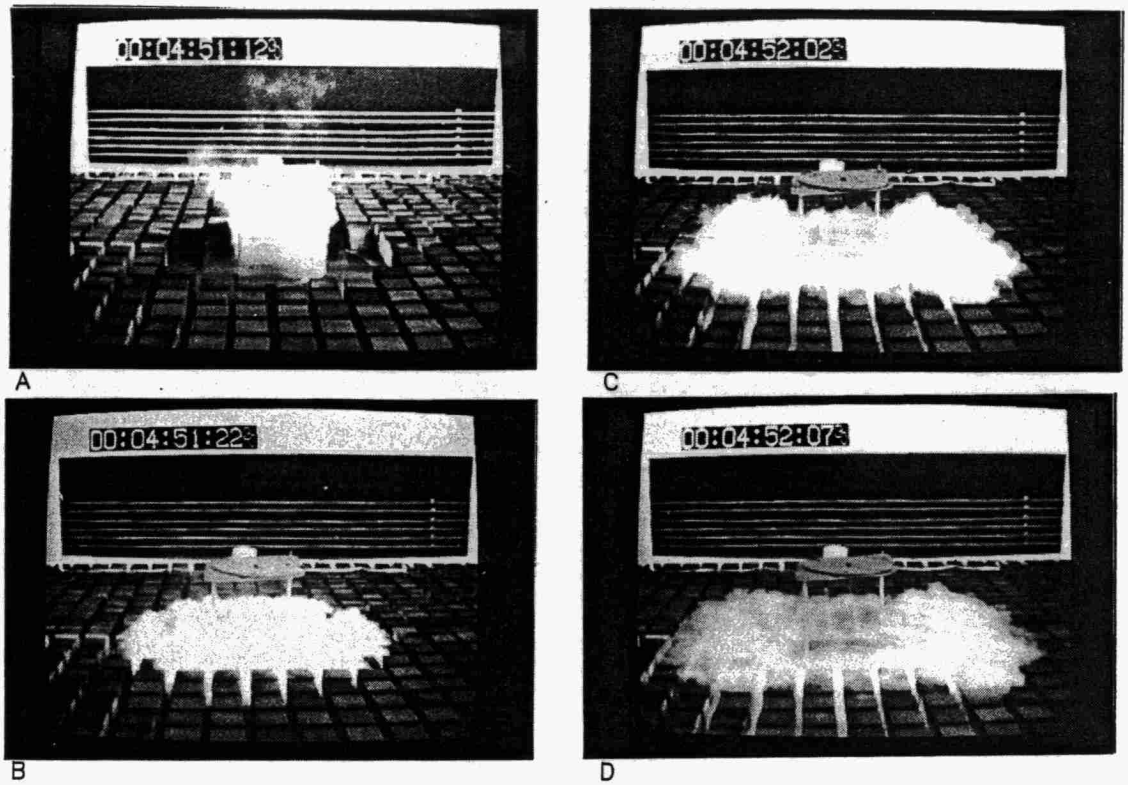

FIGURE 11
SIDE VIEW OF HEAVY GAS RELEASE – EARLY STAGES: LARGE CANISTER, MEDIUM BLOCKS, 3.5:1 SPACING, FULL COVERAGE

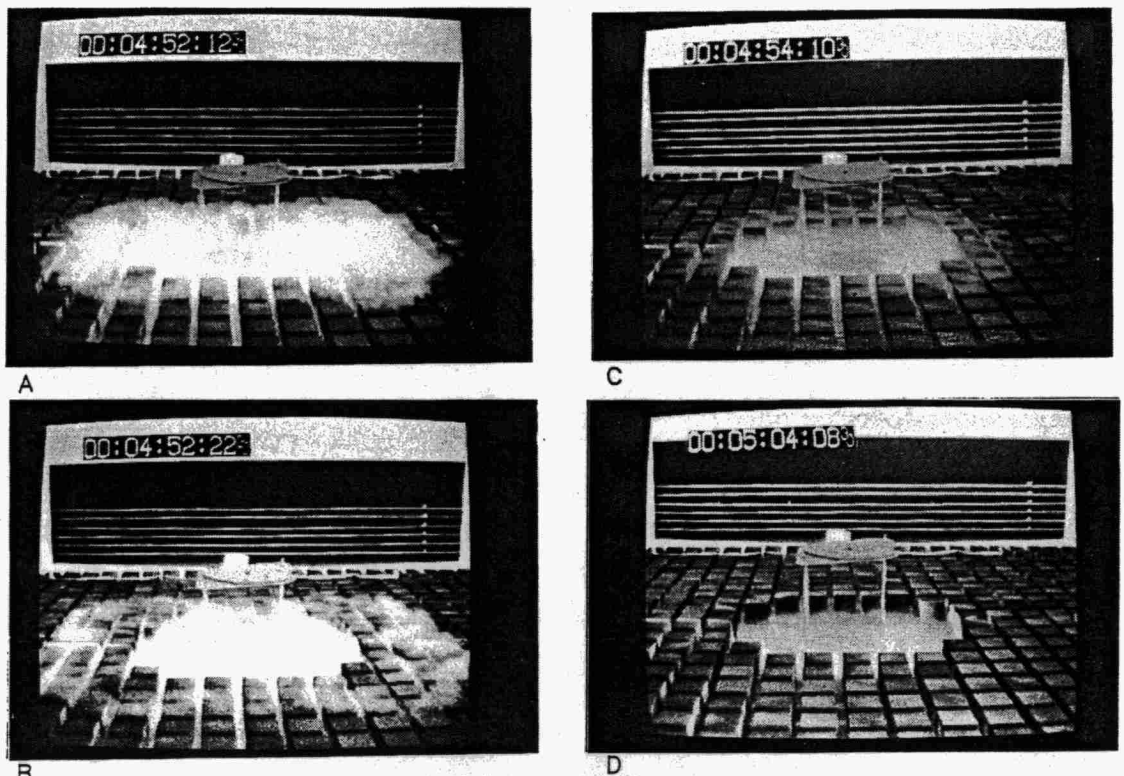

FIGURE 12
SIDE VIEW OF HEAVY GAS RELEASE – LATE STAGES: LARGE CANISTER, MEDIUM BLOCKS, 3.5:1 SPACING, FULL COVERAGE

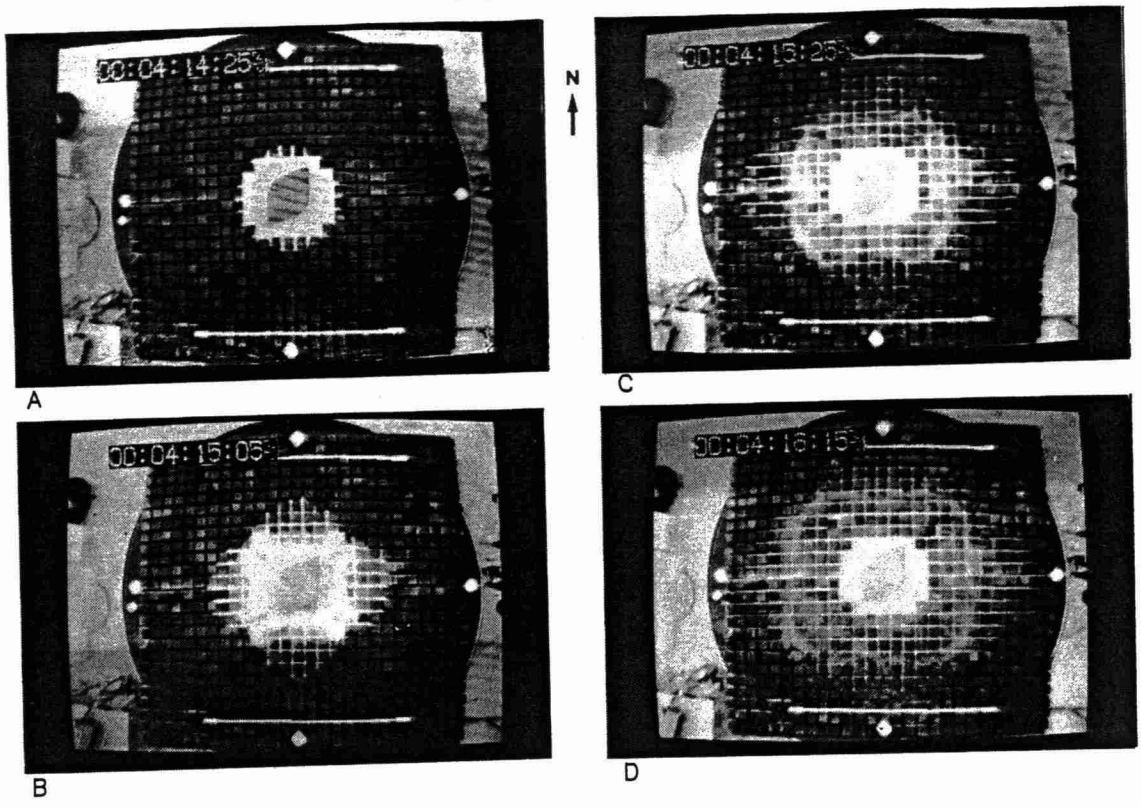

FIGURE 13
OVERHEAD VIEW OF HEAVY GAS RELEASE: LARGE CANISTER,
MEDIUM BLOCKS, 3.5:1 SPACING, FULL COVERAGE

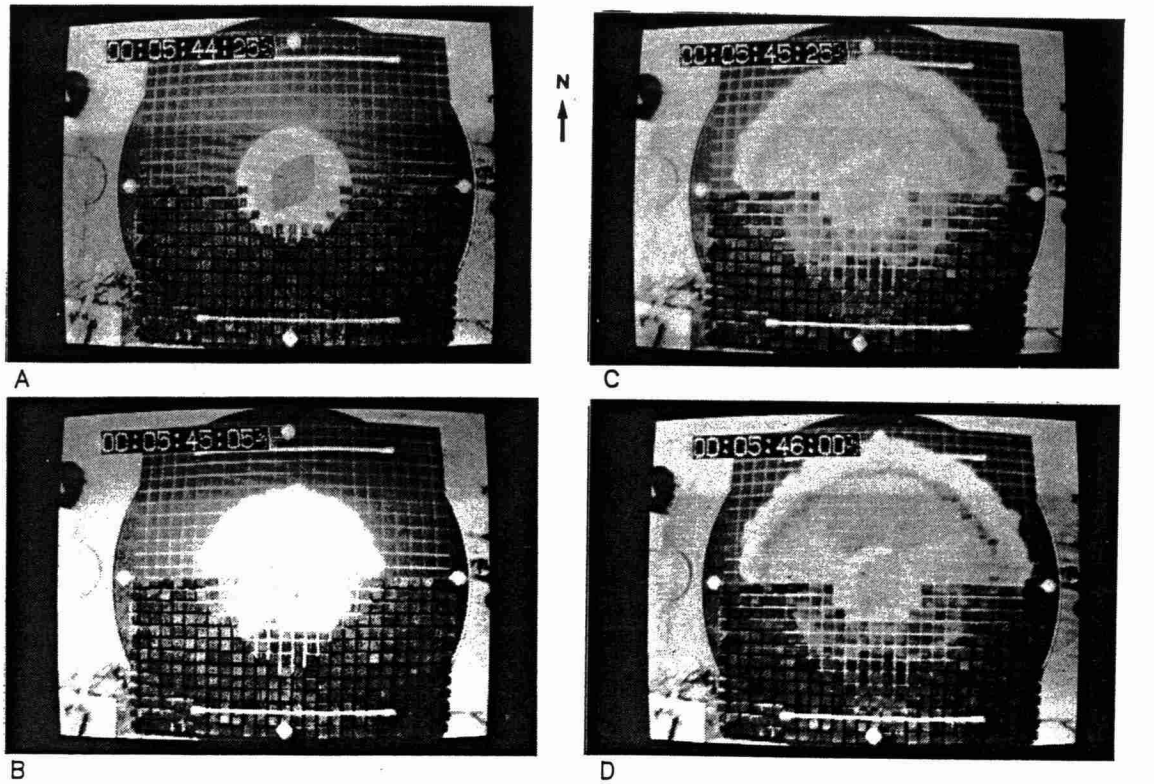

FIGURE 14
OVERHEAD VIEW OF HEAVY GAS RELEASE: LARGE CANISTER,
MEDIUM BLOCKS, 3.5:1 SPACING, HALF COVERAGE

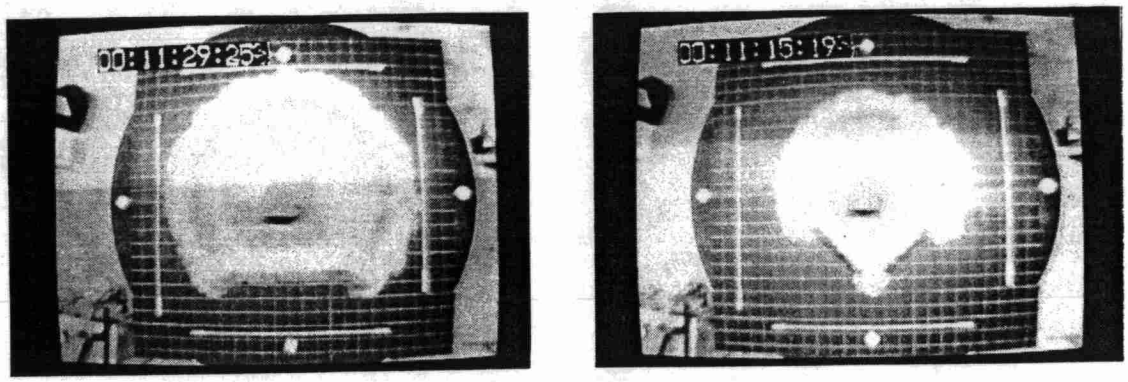

A B

FIGURE 15
OVERHEAD VIEW OF HEAVY GAS RELEASE: LARGE CANISTER
A SOLID BARRIER, B TWO BARRIERS WITH GAP

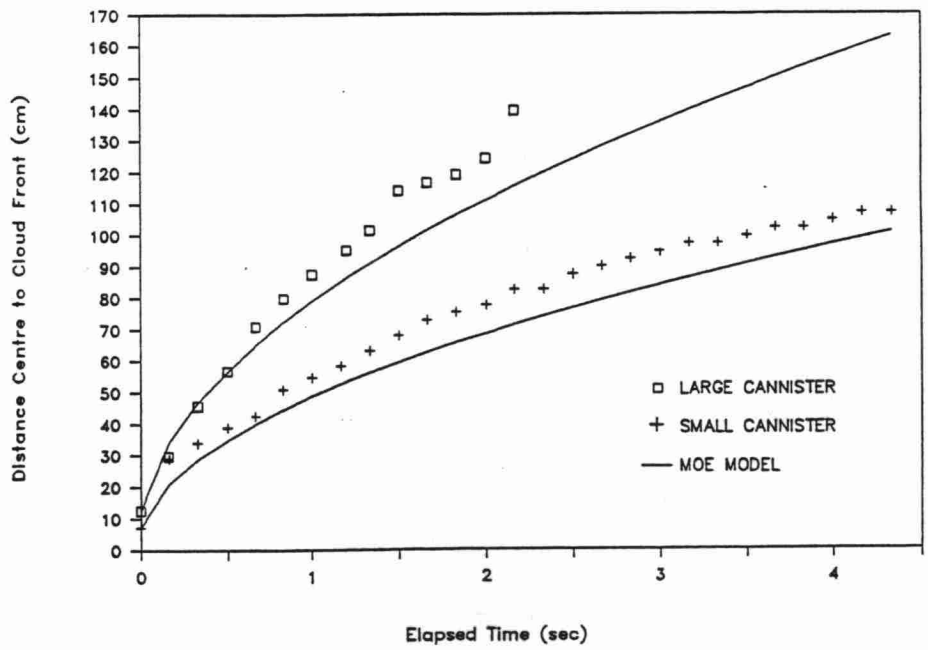

FIGURE 16
DISTANCE vs TIME: NO BLOCKS

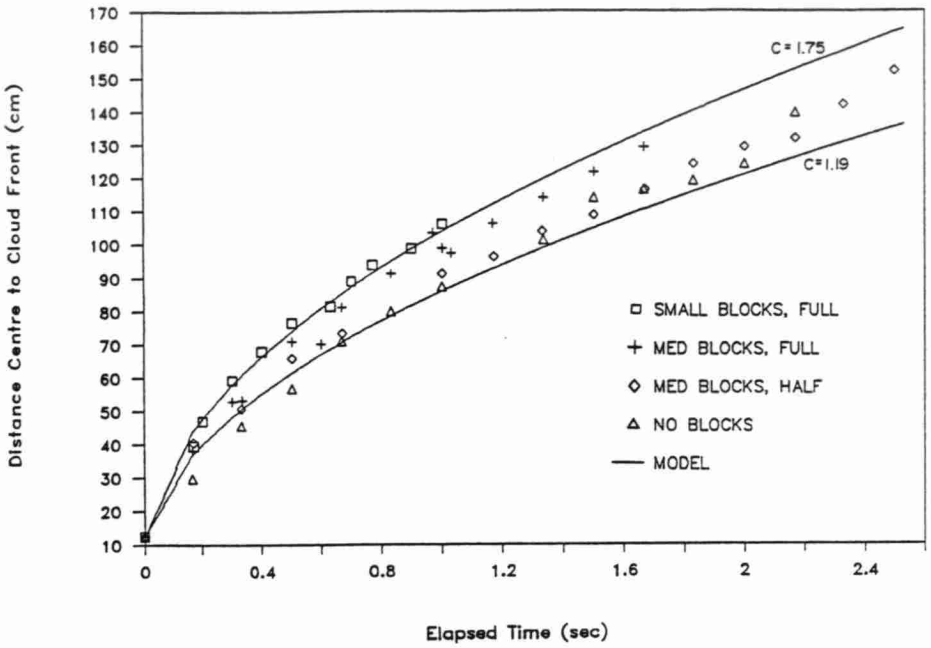

FIGURE 17
DISTANCE vs TIME: LARGE CANNISTER 90deg

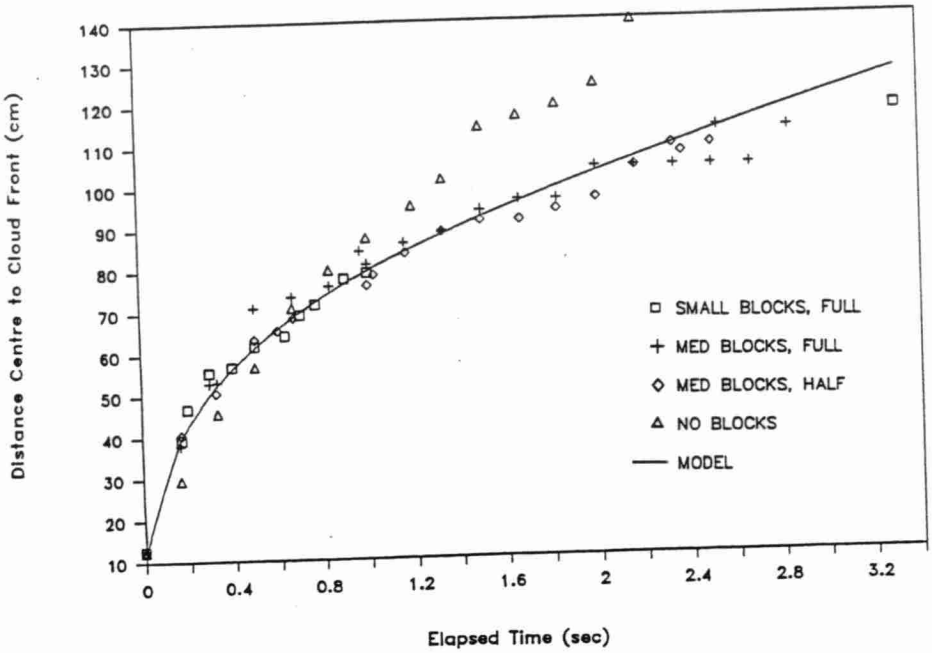

FIGURE 18
DISTANCE vs TIME: LARGE CANNISTER 45deg

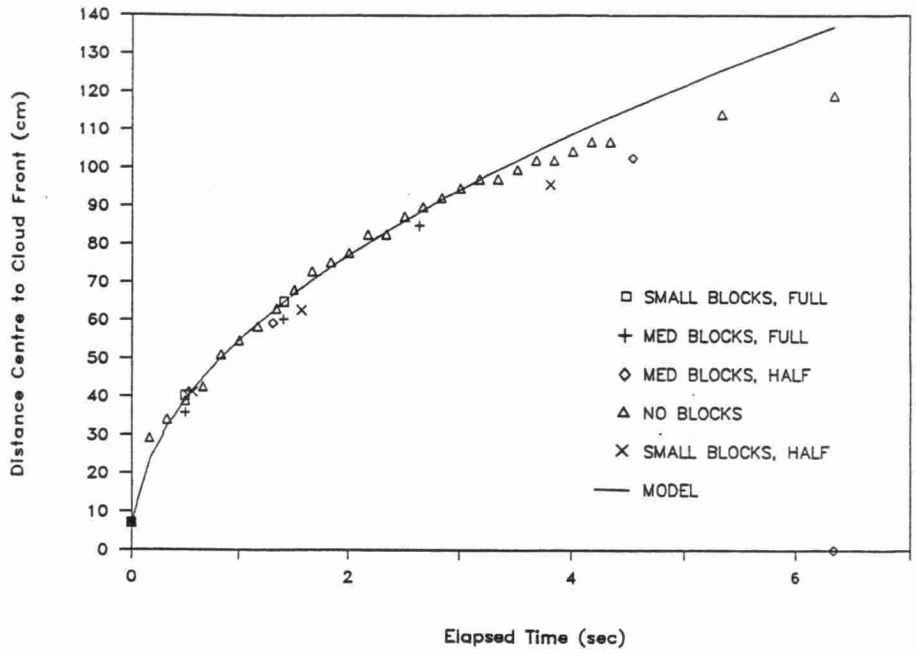

FIGURE 19
DISTANCE vs TIME: SMALL CANNISTER 90deg

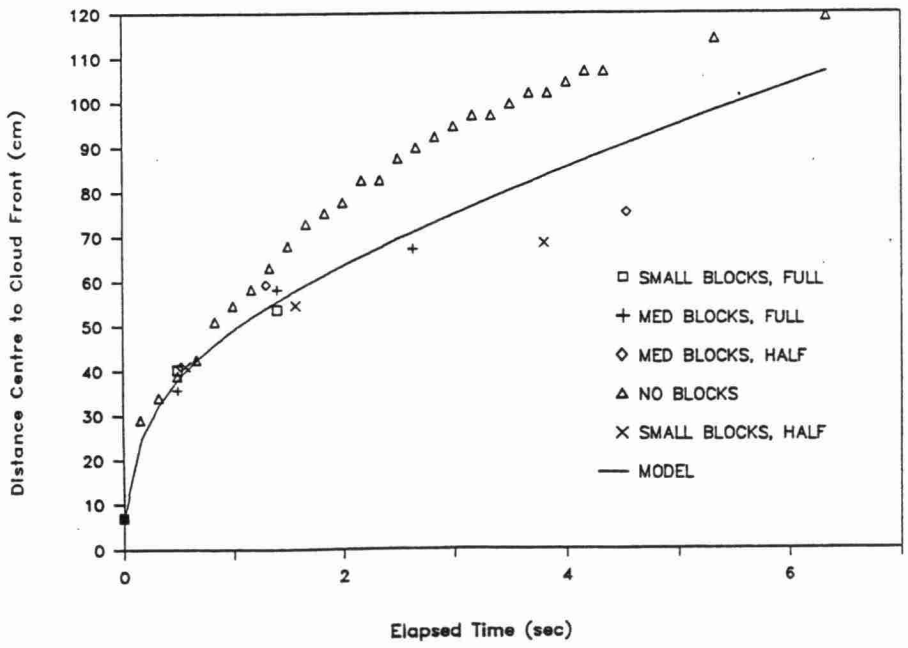

FIGURE 20
DISTANCE vs TIME: SMALL CANNISTER 45deg